ELSEVIER

Composites Science and Technology 60 (2000) 2557–2564

COMPOSITES SCIENCE AND TECHNOLOGY

www.elsevier.com/locate/compscitech

# Stress-intensity factor approximations for two-dimensional curvilinear cracks

Luigi Brandinelli [a], Roberto Ballarini [b,*]

[a] Department of Mechanical and Aerospace Engineering, Case Western Reserve University, Cleveland, OH 44106-7222, USA
[b] Department of Civil Engineering, Case Western Reserve University, Cleveland, OH 44106-7201, USA

This paper is dedicated to Dr. Nick Pagano on the occasion of his 65th birthday

**Abstract**

Two approximations are introduced and assessed that simplify the analytical and numerical treatment of curvilinear cracks in two-dimensional linear elastic fracture-mechanics analyses. The first involves the approximation of the crack trajectory with three segments that maintain a sufficiently accurate description of the near-tip geometry, including the tip's tangent. The second is associated with the use of only two segments, one of which specifies the tip's tangent. Results calculated for several configurations suggest that both approximations lead to accurate stress intensity factors and energy release rates, and can, therefore, be of great use in Monte Carlo-based characterization of random crack growth in brittle materials. An analytical expression is presented for the stress intensity factors of a curvilinear edge crack subjected to uniform far-field tension. 

## 1. Introduction

Brittle fracture is associated with tortuous crack paths, significant scatter of fracture toughness parameters, and scale effects. Recent attempts have been made to model this phenomenon by using statistical fracture mechanics (SFM) [1,2], which assumes that (1) a crack propagates along a random path of least resistance, (2) incremental propagation is governed by the Griffith energy criterion applied point-wise along the crack trajectory, and (3) the fracture energy is a random parameter that reflects, on a macroscale, the material microstructure.

SFM calculations can be conveniently performed, as described in [1], by using Monte Carlo simulations, whereby (1) the crack trajectories are simulated and the associated point-wise random (or perhaps anisotropic, with randomly orientated principal directions) fracture energy (resistance) is generated, (2) an elasticity analysis is used to calculate the crack's stress intensity factors and energy release rate as it propagates along the trajectory, (3) the energy release rate at every point is compared to the random fracture energy, and (4) statistical averaging is performed of relevant parameters such as effective fracture toughness and critical crack length.

The approach taken in [2] differs from the above in that the random fracture energy is first assigned, according to a chosen distribution, to every point in the solid, and the trajectory is determined as an output to the simulation, wherein the crack is grown incrementally and follows the path of least resistance. A schematic of a propagation increment is shown in Fig. 1, where a crack in a polycrystalline solid terminates at a grain boundary. The direction of propagation into the next crystal is determined by comparing, for each possible direction, the calculated energy release rate with the material's resistance. It should be noted that in Refs. [1,2] the elastic anisotropy of each crystal is neglected.

SFM thus relies on the capability of determining the stress intensity factors and energy release rates of curvilinear cracks in finite geometries. Since the analyses are typically performed incrementally, crack-tip parameters of piece-wise linear cracks are of particular interest. Therefore, this paper focuses on approximating stress intensity factors of cracks comprised of straight segments; it is expected that the conclusions obtained for such configurations will carry over to curved paths. Modeling the realized paths is computationally prohibitive, and certain approximations are desirable. This paper introduces two types of approximations, and quantifies the errors

* Corresponding author.

0266-3538/00/$ - see front matter 
PII: S0266-3538(00)00049-X

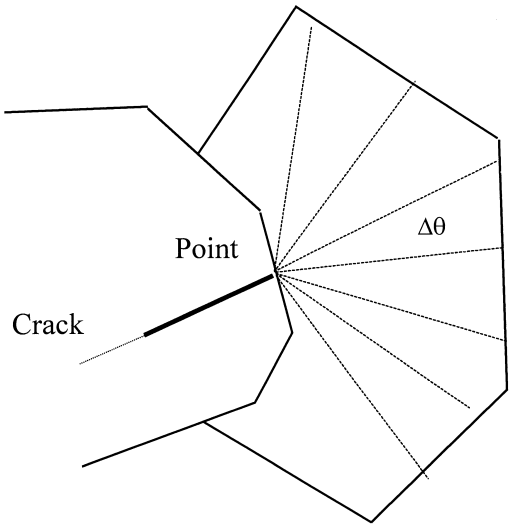


Fig. 1. A crack terminating at a grain boundary, and potential extension directions.

associated with their use through specific examples. The first involves the approximation of the actual crack path using three straight or curved segments. The second involves only two segments. The results justify the use of simplified geometries to calculate crack-tip parameters of curvilinear cracks in infinite and semi-infinite geometries, and to reduce the computational requirements needed to characterize stochastic crack propagation.

These approximations have been used in [1] and [2]. In [2], a three segment approximation to the crack trajectory is employed. Fig. 2a is a schematic of a six straight line crack trajectory initiating at point 0 and ending at point $i$. The associated three segment approximation is shown in Fig. 2b; four segments are eliminated by connecting point 0 to point $i-2$ (the segment second closest to the tip). The motivation for this approximation comes from previously calculated results [3] that suggest that the stress intensity factors and energy release rate are sensitive to only the details of the crack shape in the vicinity of the crack tip. These results are actually recalculated and presented in this paper.

In [1], a two segment approximation is employed, which, for the example in Fig. 2, would eliminate the segment second closest to the tip, and maintain only the kink that defines the crack tip's tangent by connecting point 0 to point $i-1$. This approximation, as will be illustrated in this paper through several examples, is appropriate for most configurations. However, it will also be shown through the analysis of the configuration considered in [3], that it can also lead to misleading results.

## 2. Fundamental solutions and singular integral equations

This section briefly describes the Green's function formulation of the two dimensional elastic crack ana-

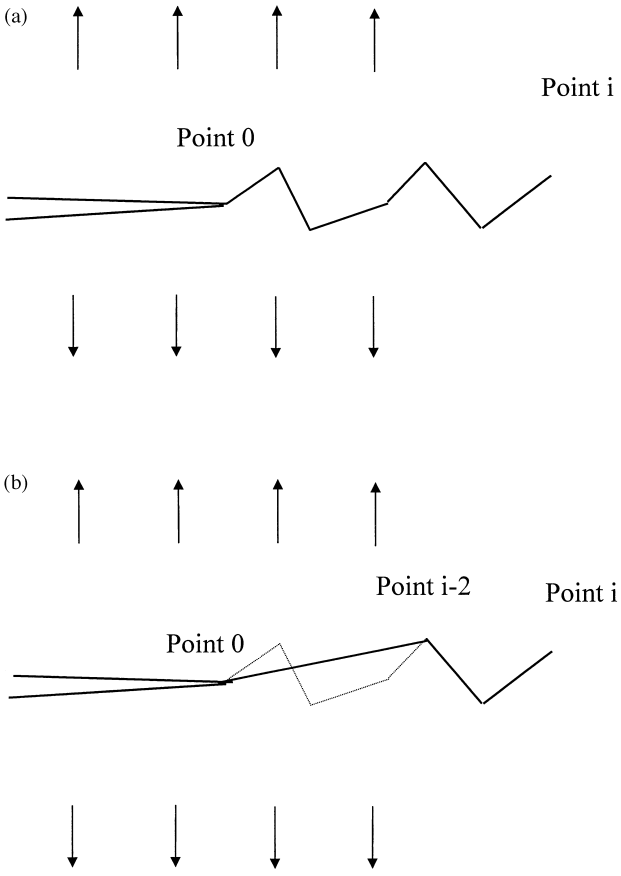


Fig. 2. (a) Incremental trajectory and (b) three segment approximation.

lyses used to calculate the crack-tip parameters of several configurations. The crack(s) is modeled as a continuous distribution of dislocations. Consider first a crack in an infinite $(x-y)$ plane. The fundamental solution represents the stress components (in the $r-\vartheta$ polar coordinate system) at a generic point $z$, within an infinite body, produced by a dislocation located at point $z_o$

$$\sigma_{\vartheta\vartheta}+i\sigma_{r\vartheta}=b\left(\frac{1}{z-z_0}+e^{2i\vartheta}\frac{\overline{z}-\overline{z_0}}{(z-z_0)^2}\right)+\overline{b}\left(\frac{1}{\overline{z}-\overline{z}_0}+\frac{e^{2i\vartheta}}{z-z_0}\right) \tag{1}$$

where $z=x+iy$, $i=\sqrt{-1}$, the complex constant $b$ is related to the Burgers vector of the dislocation $[u_r]+i[v_\vartheta]$ through

$$b=\frac{\mu([u_r]+i[v_\vartheta])e^{i\vartheta}}{\pi i(\kappa+1)} \tag{2}$$

$\kappa=3-4\nu$ for plane strain, $\kappa=(3-\nu)/(1+\nu)$ for plane stress, $\mu$ is the shear modulus, and $\nu$ is Poisson's ratio.

Introduce a continuous distribution of dislocations along the curve $\Sigma$ representing the crack, whose density

at each point is an unknown complex function $\beta(z)$, defined as

$$\beta(z_0) = \frac{\partial b}{\partial z_0} = \frac{\mu}{\pi i(\kappa+1)} \frac{\partial}{\partial z_0} \left[ e^{i\vartheta} ([u_r] + i[v_\vartheta]) \right] \tag{3}$$

where $\vartheta$ is the angle between the tangent to $\Sigma$ and the $x$-axis. Then the stress at point $z$ is symbolically given by

$$\sigma_{\vartheta\vartheta} + i\sigma_{r\vartheta} = \int_\Sigma \beta(z_0) K_1(z, z_0) \mathrm{d}z_0 + \int_\Sigma \overline{\beta(z_0)} K_2(z, z_0) \mathrm{d}\overline{z}_0 \tag{4}$$

where the kernels $K_1$ and $K_2$ are the functions that appear within the parentheses in Eq. (1). Suppose that a far-field load produces, in the uncracked solid, stress components $\sigma^\infty_{\vartheta\vartheta} + i\sigma^\infty_{r\vartheta}$ along $\Sigma$. The zero-traction condition along the crack surfaces is enforced through the Cauchy singular integral equation of the first kind

$$\int_0^{s_{\max}} \left[ \beta(s) K_1(v, s) + \overline{\beta(s)} K_2(v, s) \right] \mathrm{d}s = \sigma^\infty_{\vartheta\vartheta}(v) + i\sigma^\infty_{r\vartheta}(v) \tag{5}$$

where $v$ and $s$ are, respectively, the arc-length parameters which identify $z$ and $z_o$ along the $\Sigma$, and $s_{\max}$ is the length of the crack.

The solution to Eq. (5) is calculated using the Erdgan-Gupta method [4], which relies on certain properties of Chebyshev polynomials. To this end, Eq. (5) is normalized along the interval $(-1,1)$ and rewritten as

$$\int_{-1}^{+1} \left[ \beta(\xi) K_1(\eta, \xi) + \overline{\beta(\xi)} K_2(\eta, \xi) \right] \mathrm{d}\xi = \sigma^\infty_{\vartheta\vartheta}(\eta) + i\sigma^\infty_{r\vartheta}(\eta) \tag{6}$$

The details for calculating the relations between the integration/collocation points in the integration scheme and the arc-length parameters can be recovered in [2] and [3]. It is important to note that the formulation leads to numerical instabilities if the crack trajectory is associated with rapid changes in curvature. For a trajectory comprised of $n$ straight segments, a modification to the formulation is introduced, wherein the traction-free boundary condition along the crack is enforced through coupled integral equations for $n$ unknown dislocation densities (one for each segment), with the correct asymptotic behavior enforced at the junctions of the segments. This procedure will henceforth be referred to as the multiple integral equation method (MIEM).

If both tips of the crack are closed, a unique solution of Eq. (6) can be found by enforcing single valued displacements, i.e.

$$\int_0^{s_{\max}} \beta(s) \mathrm{d}s = 0 \tag{7}$$

Moreover, for closed cracks $\beta(\xi)$ is square root singular at both crack tips, and can be represented in the form

$$\beta(\xi) = \frac{\beta_{\mathrm{reg}}(\xi)}{\sqrt{1-\xi^2}} \tag{8}$$

where $\beta_{\mathrm{reg}}$ is a bounded function whose value at each crack tip is proportional to the stress intensity factors at that tip. For example, the nondimensionalized stress intensity factors at the right end ($s = +1$) become

$$\hat{K}_{\mathrm{II}} + i\hat{K}_{\mathrm{I}} = \frac{K_{\mathrm{II}} + iK_{\mathrm{I}}}{\sigma^\infty_{xx}\sqrt{\pi s_{\max}/2}} = -2\pi \left[ \frac{i\beta_{\mathrm{reg}}(+1)}{e^{i\vartheta_0}} \right] \tag{9}$$

where $s_{\max}$ is the crack length, and $\vartheta_0$ is the angle between the tangent at the crack-tip and the $x$-axis.

For a semi-infinite crack, the zero-traction condition renders the singular integral equation homogeneous, and is satisfied by all functions of the type

$$\beta(s) = C \frac{\beta_{\mathrm{reg}}(s)}{\sqrt{-s}} \tag{10}$$

where $C$ is a constant and $s$ is the arc-length measured from the crack-tip. In this case a far-field loading is introduced by writing the unknown dislocation density as

$$\beta(s) = \frac{\beta_{\mathrm{reg}}(s)}{\sqrt{-s}} - \frac{K^\infty_{\mathrm{I}} \left( 1 - e^{-s^2} \right)}{2\pi i \sqrt{-2\pi s}} \tag{11}$$

The first term on the right hand side of Eq. (11) takes care of the square root singularity at the crack-tip, while the second term guarantees that the crack opening displacements are consistent with those produced by the nominal stress intensity $K^\infty_{\mathrm{I}}$. Again the normalized stress intensity factors are proportional to the regular part of the dislocation density

$$\hat{K}_{\mathrm{II}} + i\hat{K}_{\mathrm{I}} = \frac{K_{\mathrm{II}} + iK_{\mathrm{I}}}{K^\infty_{\mathrm{I}}} = (2\pi)^{3/2} \left[ \frac{i\beta_{\mathrm{reg}}(s=0)}{e^{i\vartheta_0}} \right] \tag{12}$$

A similar procedure can be used for cracks in semi-infinite planes (edge-cracks, for example). The fundamental solution in this case is a dislocation in a half-plane, and the kernels $K_1$ and $K_2$ in Eqs. (4)–(6) are replaced, respectively, with the terms within the parentheses in the following equation

$$\begin{aligned} \sigma_{\vartheta\vartheta} + i\sigma_{r\vartheta} = b \Bigg\{ & \frac{1}{z - z_0} - \frac{1}{z - \overline{z}_0} - \frac{1}{\overline{z} - z_0} + \frac{\overline{z} - \overline{z}_0}{(\overline{z} - z_0)^2} \\ & + e^{2i\vartheta} \left[ \frac{\overline{z} - z}{(z - \overline{z}_0)^2} + \frac{1}{z - \overline{z}_0} + \frac{\overline{z}_0 - \overline{z}}{(z - z_0)^2} \right] \Bigg\} \\ & + \overline{b} \Bigg\{ - \frac{1}{z - \overline{z}_0} + \frac{1}{\overline{z} - \overline{z}_0} - \frac{1}{\overline{z} - z_0} + \frac{z - z_0}{(z - \overline{z}_0)^2} \\ & + e^{2i\vartheta} \left[ \frac{2(\overline{z} - z)}{(z - \overline{z}_0)^2} + \frac{2(\overline{z} - z)(z_0 - z)}{(z - \overline{z}_0)^3} + \frac{z_0 - z}{(z - \overline{z}_0)^2} + \frac{1}{z - z_0} \right] \Bigg\} \end{aligned} \tag{13}$$

The stress intensity factors at the tip ($s = +1$) are given by

$$\hat{K}_{\mathrm{II}} + i\hat{K}_{\mathrm{I}} = \frac{K_{\mathrm{II}} + iK_{\mathrm{I}}}{\sigma_{xx}^{\infty}\sqrt{\pi s_{\max}}} = -\frac{2\pi}{\sqrt{2}}\left[\frac{i\beta_{\mathrm{reg}}(+1)}{\mathrm{e}^{i\vartheta_0}}\right] \tag{14}$$

## 3. Results

### 3.1. Semi-infinite crack with sinudoidal near-tip shape, in infinite plane, under mode-I loading

The configuration of the first problem considered is shown in Fig. 3. A semi-infinite crack with a sinusoidal near-tip shape is loaded by a far-field stress intensity factor $K_{\mathrm{I}}^{\infty}$. This problem was solved in [3] using the procedures described above. As discussed subsequently, it was the results calculated for this geometry that suggested that stress intensity factors of curvilinear cracks can be estimated with sufficient accuracy by describing only the details of the near-tip region. This problem is recalculated here to check the numerical solution algorithm and to further explore the physical results.

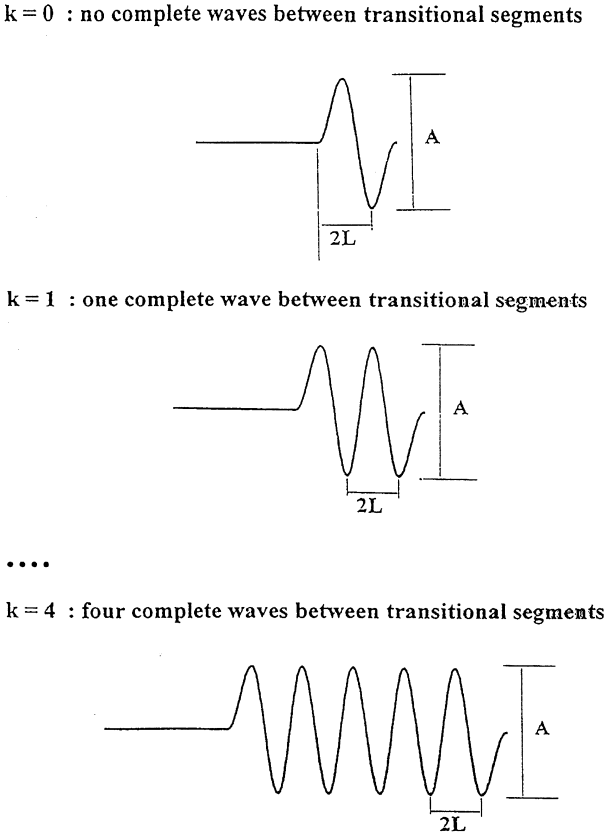


Fig. 3. Semi-finite crack with sinusoidal near-tip under nominal mode-I loading.

The number of complete waves is $k$. Two transitional segments are introduced, the first to connect the waves to the main crack, the second to maintain a horizontal tangent at the tip of the crack. The fact that the tip's tangent is aligned with the main crack will be revisited later. The coordinates of the crack are defined through the equations

$$y = \frac{A}{2}\begin{cases} \cos\left(\dfrac{\pi x}{L}\right) - 1 & -L < x < 0 \\ \cos\left(\dfrac{\pi x}{L}\right) & -(2k+2)L < x < -L \\ \cos\left(\dfrac{\pi x}{L}\right) + 1 & -(2k+3)L < x < -(2k+2)L \end{cases} \tag{15}$$

and thus stress intensity factors and energy release rate, normalized with respect to the applied values, depend only on $k$ and $A/L$. The calculated crack-tip parameters presented henceforth are normalized with respect to the far-field values.

Fig. 4 illustrates, for $k = 0$ and $A/L = 2$, the fluctuation of the energy release rate as the crack-tip moves along its curvilinear path. Also shown is the average energy release rate $G_{\mathrm{av}}$. It is observed that for this case there is a reduction of more than fifty percent in crack-tip driving force. Qualitatively similar results (not shown here) were calculated for other $k$ and $A/L$ values. Fig. 5 shows, for $k = 0$, the dependence on $A/L$ of the stress intensity factors and energy release rate as the crack crosses the $x$-axis. Recall that in this position the crack tip has a horizontal tangent. It is clear that the crack shape can significantly effect the crack-tip parameters. However, as shown in Table 1 (for $A/L = 1$), the crack-tip parameters do not depend on the number of waves. As mentioned previously, this result motivated the previously described three segment approximation in [2].

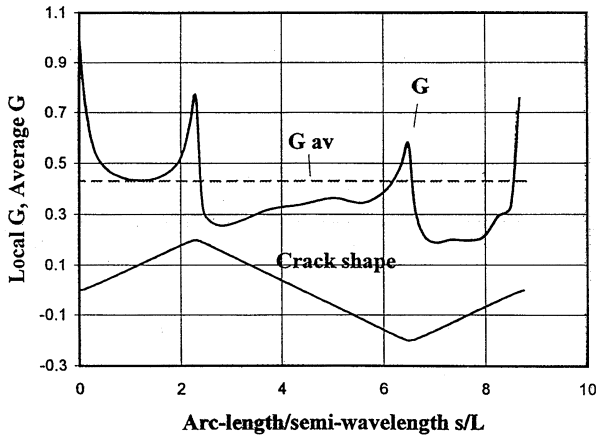


Fig. 4. Energy release rate of mode-I loaded semi-infinite crack with sinusoidal near-tip shape, $k = 0$, $A/L = 2$.

Fig. 5, which is associated with 500 integration points in the Erdogan–Gupta method (and using double precision on a Sun Ultra-2 work station), also illustrates that the numerical calculations become unstable for relatively large values of $A/L$. In [3] the calculations were performed using a computer whose precision is approximately double that used here, and the instabilities were not observed (private communication with A.A. Rubinstein).

This specific example also demonstrates that a two segment approximation can lead to misleading results. Indeed, the two segment approximation to this problem, as used in [1], would reduce the geometry to a straight semi-infinite crack (one long segment that represents the main crack, and one short segment that represents the horizontal tip tangent), and the effects of near-tip shape would be completely missed! On the other hand, the three segment approximation would consist of a semi-infinite crack (the first segment), a transition wave (the second), and a horizontal tip (the third). Table 1 justifies the approximation.

The following result is new. The calculated results essentially provide the ratio of crack-tip energy release rate to applied energy release rate

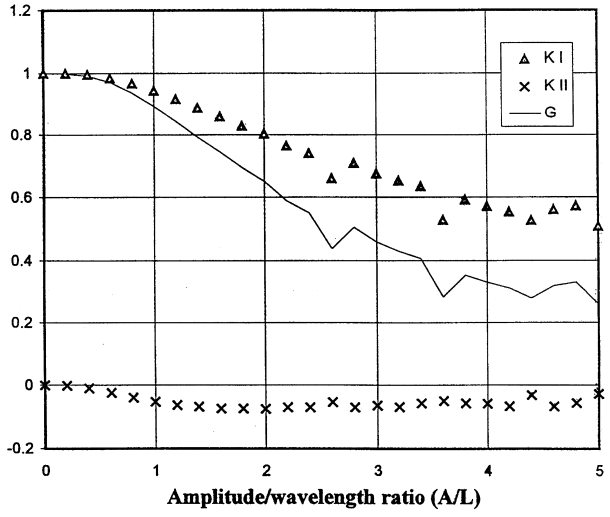


Fig. 5. Crack-tip parameters for mode-I loaded semi-infinite crack with sinusoidal near-tip shape, $k = 0$.

Table 1
Stress intensity factors for mode-I loaded semi-infinite crack with sinusoidal near-tip shape, $A/L = 1$

| $k$ | $K_I/K_I^\infty$ | $K_{II}/K_{II}^\infty$ |
|---|---|---|
| 1 | 0.94 | −0.052 |
| 2 | 0.94 | −0.055 |
| 3 | 0.95 | −0.054 |
| 4 | 0.95 | −0.051 |
| 5 | 0.95 | −0.054 |

$$F(s) \equiv \frac{G}{G^\infty} \tag{16}$$

where $s$ is the arc-length parameter that defines the position of the crack-tip. Assume that the intrinsic fracture energy is a constant $G_{Ic}$. Then the reciprocal of function $F$, shown in Fig. 6 for $k = 1$ and selected values of $A/L$, represents the normalized applied energy release rate that is in equilibrium with the crack-tip position. Furthermore, the peak of this function is a measure of the apparent toughness increase that results from the tortuous path, defined by $A/L$. As shown in Fig. 7, amazingly the crack-path toughening follows, with sufficient accuracy, the relation

$$\frac{G^\infty_{\text{critical}}}{G_{Ic}} = e^{A/L} \tag{17}$$

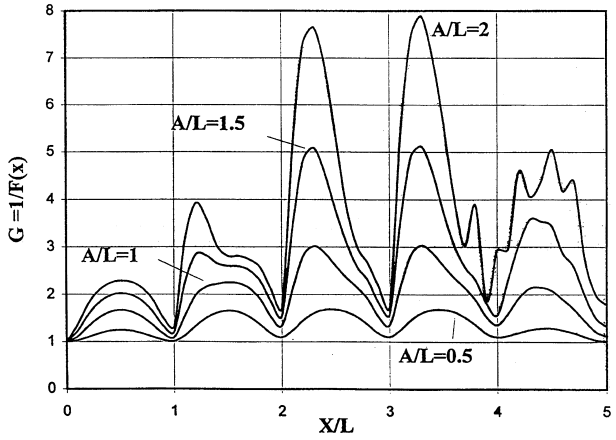


Fig. 6. Energy release rate of mode-I loaded semi-infinite crack with sinusoidal near-tip shape that is in equilibrium with crack-tip position, $k = 1$.

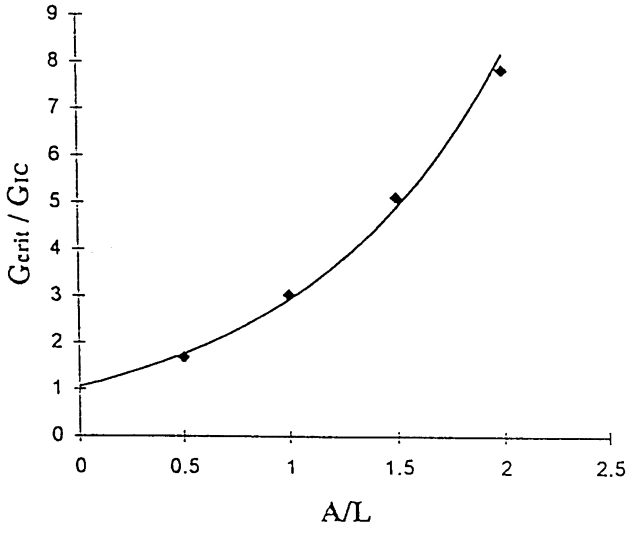


Fig. 7. Crack-path toughening of mode-I loaded semi-infinite crack with sinusoidal near-tip shape,.

### 3.2. Kinked inclined edge-crack in a semi-infinite plane under uniform far-field tension

The accuracy of the MIEM is assessed through the inclined kinked edge crack under uniform far-field tension, shown in Fig. 8. Table 2 compares, for $\Theta_1 = 90^\circ$, the calculated (using 50 integration points) normalized stress intensity factors

$$F_{\mathrm{I}} = \frac{K_{\mathrm{I}}}{\sigma\sqrt{\pi b}} \quad F_{\mathrm{II}} = \frac{K_{\mathrm{II}}}{\sigma\sqrt{\pi b}} \tag{18}$$

with those presented in [5] (as calculated in [6] using a body force method). It is observed that the agreement is excellent, and provides confidence in the treatment of the discontinuous tangent at the junction of the straight line segments. An additional check is provided next for cases where the number of segments is relatively large.

### 3.3. Zig-zag edge crack in semi-infinite plane under uniform far-field tension; two and three segment approximation

Fig. 9(a) shows a zig-zag edge-crack, comprised of $N$ segments, in a semi-infinite plane subjected to a remote uniform stress parallel to the edge. The two and three segment approximations to this geometry are shown, respectively, in Fig. 9(b) and (c). The normalized stress intensity factors

$$G_{\mathrm{I}} = \frac{K_{\mathrm{I}}}{\sigma\sqrt{\pi N a}} \quad G_{\mathrm{II}} = \frac{K_{\mathrm{II}}}{\sigma\sqrt{\pi N a}} \tag{19}$$

calculated using the approximate geometries are compared in Tables 3 and 4 with those of the actual trajectory, presented in [5] (as calculated in [7] using a body-force method). For $N = 5$, the stress intensity factors of the actual configuration were also calculated using the MIEM, and are presented in parentheses. It is observed that both approximations are associated with relatively small errors. However, recall that the two segment approximation can, as discussed previously, lead to misleading results.

### 3.4. Inclined zig-zag edge crack

The previous example is associated with a crack whose plane, on the average, is perpendicular to the applied stress. To investigate the effects of an average plane not perpendicular to the applied stress, results for the inclined zig-zag crack shown in Fig. 10 are presented, for $\theta = 60^\circ$ in Table 5. It is observed that the approximate stress intensity factors are in excellent

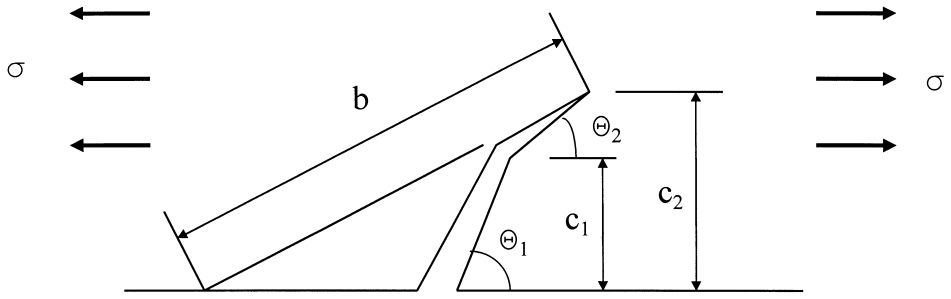


Fig. 8. A kinked inclined edge-crack in a semi-infinite plane under uniform tension.

Table 2
Stress intensity factors of kinked edge-crack ($\Theta_1 = 90$)

| $\Theta_2$ (deg.) | $c_1$ | $c_2$ | $F_{\mathrm{I}}$ | $F_{\mathrm{II}}$ | $F_{\mathrm{I}}$ [5] | $F_{\mathrm{II}}$ [5] |
|---|---|---|---|---|---|---|
| 30 | 0.25 | 1.0 | 0.462 | 0.336 | 0.459 | 0.338 |
| 45 | 0.25 | 1.0 | 0.705 | 0.365 | 0.703 | 0.365 |
| 60 | 0.25 | 1.0 | 0.920 | 0.306 | 0.919 | 0.306 |
| 30 | 0.5 | 1.0 | 0.463 | 0.337 | 0.463 | 0.337 |
| 45 | 0.5 | 1.0 | 0.705 | 0.365 | 0.704 | 0.365 |
| 60 | 0.5 | 1.0 | 0.920 | 0.306 | 0.919 | 0.306 |
| 30 | 0.75 | 1.0 | 0.463 | 0.340 | 0.465 | 0.340 |
| 45 | 0.75 | 1.0 | 0.705 | 0.365 | 0.705 | 0.366 |
| 60 | 0.75 | 1.0 | 0.920 | 0.304 | 0.919 | 0.304 |
| 30 | 0.9 | 1.0 | 0.464 | 0.339 | 0.468 | 0.342 |
| 45 | 0.9 | 1.0 | 0.706 | 0.357 | 0.707 | 0.359 |
| 60 | 0.9 | 1.0 | 0.921 | 0.295 | 0.921 | 0.296 |

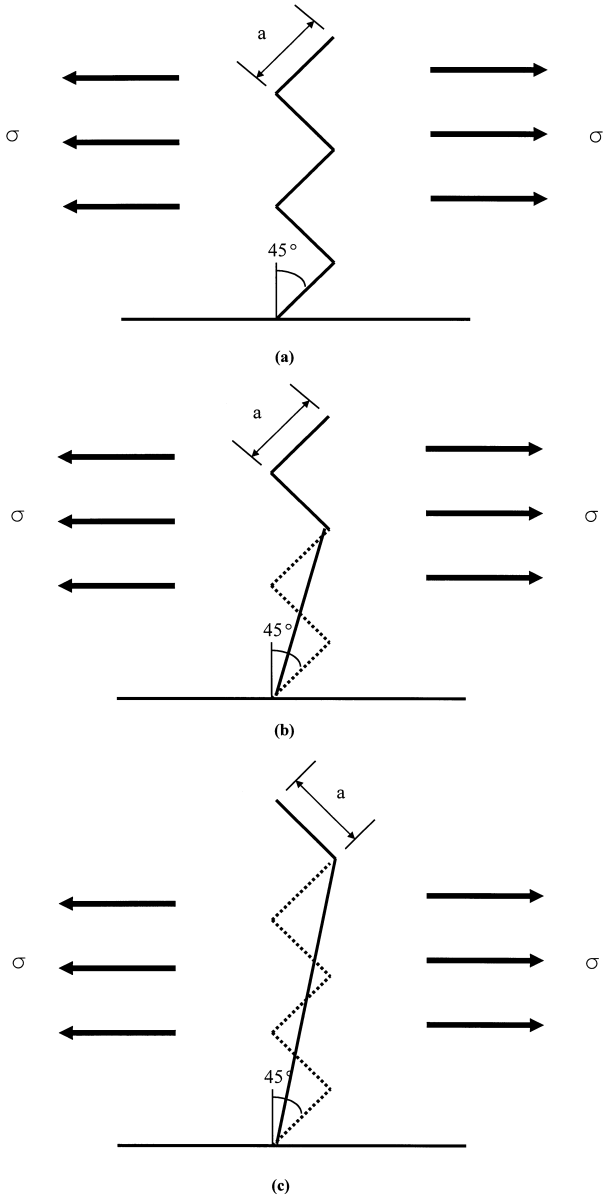


Fig. 9. (a) Zig-zag edge-crack in semi-infinite plane under uniform tension; (b) three segmented approximation; (c) two segment approximation.

Table 3
Normalized stress intensity factors of a zig-zag edge-crack: three segment approximation

| $N$ | $G_I$ | $G_{II}$ | $G_I$ [5] (MIEM) | $G_{II}$ [5] (MIEM) |
|---|---|---|---|---|
| 4 | 0.709 | 0.353 | 0.704 | 0.355 |
| 5 | 0.702 | −0.343 | 0.708 (0.711) | −0.349 (−0.348) |
| 6 | 0.714 | 0.344 | 0.707 | 0.348 |
| 7 | 0.711 | −0.339 | | |
| 8 | 0.718 | 0.338 | | |
| 9 | 0.717 | −0.335 | | |
| 10 | 0.722 | 0.333 | | |

Table 4
Normalized stress intensity factors of a zig-zag edge-crack: two segment approximation

| $N$ | $G_I$ | $G_{II}$ | $G_I$ [5] | $G_{II}$ [5] |
|---|---|---|---|---|
| 3 | 0.705 | −0.366 | 0.704 | −0.360 |
| 4 | 0.705 | 0.363 | 0.704 | 0.355 |
| 5 | 0.705 | −0.365 | 0.708 | −0.349 |
| 6 | 0.706 | 0.360 | 0.707 | 0.348 |
| 7 | 0.706 | −0.363 | | |
| 8 | 0.707 | 0.357 | | |
| 9 | 0.707 | −0.360 | | |
| 10 | 0.708 | 0.355 | | |

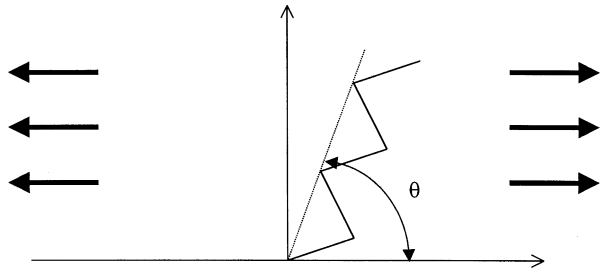


Fig. 10. Inclined zig-xag edge-crack in semi-infinite plane under uniform tension; results calculated for $\theta = 60°$.

Table 5
Normalized stress intensity factors of inclined zig-zag edge-crack: two and three segment, approximations

| $N$ | $G_I$ (MIEM) | $G_{II}$ (MIEM) | $G_I$ (two segment) | $G_{II}$ (two segment) | $G_I$ (three segment) | $G_{II}$ (three segment) |
|---|---|---|---|---|---|---|
| 5 | 0.341 | −0.346 | 0.343 | −0.355 | 0.340 | −0.345 |

agreement with those of the actual configuration, which were calculated using the MIEM.

## 4. Conclusions

Approximations have been introduced that simplify calculations of stress intensity factors and energy release rates of curvilinear cracks in infinite and semi-infinite two dimensional configurations. The results calculated for specific examples associated with piece-wise linear cracks suggest that two and three segment approximations of a crack path are highly accurate, and could be used to reduce the computations needed to characterize, using Monte Carlo techniques, random crack propagation in brittle materials.

In fact, the two segment approximation can be used, as follows, to obtain an analytic expression for the stress intensity factors of an arbitrarily shaped edge crack

under uniform far-field tension. Define the crack path through function $y(x)$, where $x$ is perpendicular to the free surface, defined by $x = 0$. Note that at any point along the crack path, $(x_0, y_0)$, the tip's tangent is defined by $\tan\theta = y'(x_0)$. The stress intensity factors of a straight inclined edge crack under uniform tension are given by [5]

$$K_{\mathrm{I}}^{*} = H_{\mathrm{I}}(\beta)\sigma\sqrt{\pi a} \tag{20}$$

$$K_{\mathrm{II}}^{*} = H_{\mathrm{II}}(\beta)\sigma\sqrt{\pi a} \tag{21}$$

where $\beta$ represents the angle which the crack makes with the free surface, and functions $H_{\mathrm{I}}$ and $H_{\mathrm{II}}$ are tabulated in [5] (these can be easily converted to polynomials). This edge crack is used as the first of the two segments in the two segment approximation. Therefore at any point along the crack path, $\tan\beta = x_0/y_0$. The second segment is now taken as a small kink orientated at an angle $\theta$ with respect to the original direction; the stress intensity factors of this extension can be approximated by [8]

$$K_{\mathrm{I}}(\beta,\theta) = \frac{1}{4}\left(3\cos\frac{\theta}{2} + \cos\frac{3\theta}{2}\right)K_{\mathrm{I}}^{*} - \frac{3}{4}\left(\sin\frac{\theta}{2} + \sin\frac{3\theta}{2}\right)K_{\mathrm{II}}^{*} \tag{22}$$

$$K_{\mathrm{II}}(\beta,\theta) = \frac{1}{4}\left(\sin\frac{\theta}{2} + \sin\frac{3\theta}{2}\right)K_{\mathrm{I}}^{*} + \frac{1}{4}\left(\cos\frac{\theta}{2} + 3\cos\frac{3\theta}{2}\right)K_{\mathrm{II}}^{*} \tag{23}$$

Eqs. (22) and (23) are proposed as the stress intensity factors of an arbitrarily shaped curvilinear crack. The authors are currently assessing the accuracy of these approximations.

## Acknowledgements

This research was funded by the National Science Foundation under Grants MSS94-16752 and CMS97-13997, and by ARPA under Grant DABT 63-92-C-0032.

## References

[1] Chudnovsky A, Gorelik M. Tortuousity of crack path, fracture toughness and scale effect in brittle fracture. In: Carpinteri A, editor. Size-scale effects in the failure mechanisms of materials and structures. London: E&FN Spon, 1996. p. 97–108.
[2] Brandinelli L. Characterization of planar curvilinear cracks and development of a probabilistic crack propagation model for brittle materials. M.S. thesis, Department of Mechanical and Aerospace Engineering, Case Western Reserve University, August 1997.
[3] Rubinstein AA. Crack-path effect on material toughness. ASME Journal of Applied Mechanics 1990;57:97–103.
[4] Erdogan F, Gupta GD. On the numerical solution of singular integral equations. Quarterly Journal of Applied Mathematics 1972;29:525–34.
[5] Murakami Y, editor. Stress intensity factor handbook, volume 1. Oxford: Pergamon Press, 1987 (pp. 120–1).
[6] Nisitani H. Stress intensity factor for the tension of a semi-infinite plate having an oblique or a bent edge crack. Trans Japan Soc Mech Engrs 1975;41(344):1103–10.
[7] Isida M. Tension of a half plane containing array cracks, branched cracks and cracks emanating from sharp notches. Trans Japan Soc Mech Engrs 1979;45(392):306–17.
[8] Cotterell B, Rice JR. Slightly curved or kinked cracks. International Journal of Fracture 1980;16:155–69.